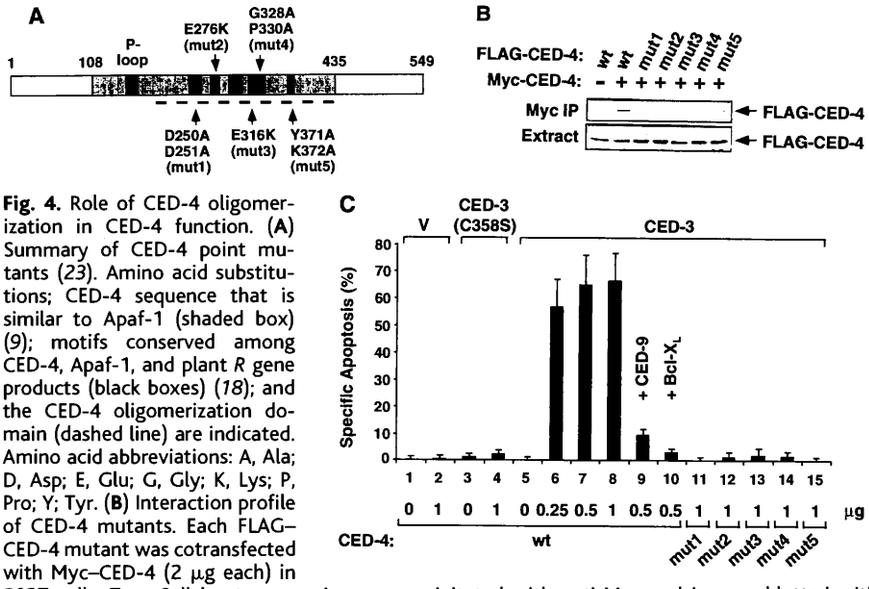

Fig. 4. Role of CED-4 oligomerization in CED-4 function. (**A**) Summary of CED-4 point mutants (*23*). Amino acid substitutions; CED-4 sequence that is similar to Apaf-1 (shaded box) (*9*); motifs conserved among CED-4, Apaf-1, and plant *R* gene products (black boxes) (*18*); and the CED-4 oligomerization domain (dashed line) are indicated. Amino acid abbreviations: A, Ala; D, Asp; E, Glu; G, Gly; K, Lys; P, Pro; Y; Tyr. (**B**) Interaction profile of CED-4 mutants. Each FLAG–CED-4 mutant was cotransfected with Myc–CED-4 (2 μg each) in 293T cells. Top: Cell lysates were immunoprecipitated with anti-Myc and immunoblotted with anti-FLAG as in Fig. 2B. Bottom: Immunoblot of 5% of input IP extract. (**C**) Pro-apoptotic activity of CED-4 mutants. HeLa cells were transfected with indicated amount of CED-4 or CED-4 mutants; 50 ng of vector (lanes 1 and 2), CED-3(C358S) (lanes 3 and 4), or CED-3 (lanes 5 to 15); 1 μg of CED-9 (lane 9) or Bcl-x_L (lane 10); and 0.25 μg of pCMV-lacZ. Cells were stained 16 hours after transfection and scored for specific apoptosis (*25*). Data shown (mean ± SD) are from at least three independent experiments, and in each experiment more than 300 blue cells were counted; wt, wild type.

tion. Mammalian Apaf-1 can also oligomerize and may function in a similar way to activate pro–caspase-9. In this model, the activation of CED-9–binding activity of a pro-apoptotic protein upstream of the apoptosome is a key event and requires further investigation. Additional regulators, such as dATP and cytochrome c (*21*), may control apoptosome function through similar or distinct mechanisms.

Note added in proof: It was recently shown that Apaf-1 can form oligomers and may activate pro–caspase-9 molecules by oligomerizing them (*22*).

References and Notes

1. H. Steller, *Science* **267**, 1445 (1995).
2. H. R. Horvitz, S. Shaham, M. O. Hengartner, *Cold Spring Harbor Symp. Quant. Biol.* **LIX**, 377 (1994).
3. A. M. Chinnaiyan *et al.*, *Science* **275**, 1122 (1997).
4. D. Wu, H. D. Wallen, G. Nuñez, *ibid.*, p. 1126.
5. M. S. Spector *et al.*, *Nature* **385**, 653 (1997).
6. M. O. Hengartner, *ibid.* **388**, 714 (1997).
7. J. Yuan *et al.*, *Cell* **75**, 641 (1993).
8. M. O. Hengartner and H. R. Horvitz, *ibid.* **76**, 665 (1994).
9. H. Zhou, W. I. Henzel, X. Liu, A. Luschg, X. Wang, *ibid.* **90**, 405 (1997); P. Li *et al.*, *ibid.* **91**, 479 (1997).
10. X. Yang, H. Y. Chang, D. Baltimore, *Mol. Cell* **1**, 319 (1998).
11. M. Muzio, B. R. Stockwell, H. R. Stennicke, G. S. Salvesen, V. M. Dixit, *J. Biol. Chem.* **273**, 2926 (1998).
12. H. Steller, *Proc. Natl. Acad. Sci. U.S.A.* **95**, 5421 (1998).
13. J. F. Amara *et al.*, *ibid.* **94**, 10618 (1997).
14. S. Ottilie *et al.*, *Cell Death Differ.* **4**, 526 (1997).
15. A. M. Chinnaiyan, D. Chaudhary, K. O'Rourke, E. V. Koonin, V. M. Dixit, *Nature* **388**, 728 (1997).
16. S. Shaham and H. R. Horvitz, *Cell* **86**, 201 (1996).
17. Y. Hu, M. A. Benedict, D. Wu, N. Inohara, G. Nunez, *Proc. Natl. Acad. Sci. U.S.A.* **95**, 4386 (1998).
18. E. A. van der Biezen and J. D. G. Jones, *Curr. Biol.* **8**, R226 (1998).
19. Each FLAG–CED-4 mutant was cotransfected with AU1–CED-3(C358S) into 293T cells. Cell lysates were immunoprecipitated with antibody to AU1 (anti-AU1) (Babco) and immunoblotted with anti-FLAG. Each CED-4 mutant interacted with CED-3(C358S) as well as wild-type CED-4.
20. B. Conradt and H. R. Horvitz, *Cell* **93**, 519 (1998).
21. X. Liu, C. N. Kim, J. Yang, R. Jemmerson, X. Wang, *ibid.* **86**, 147 (1996).
22. S. M. Srinivasula *et al.*, *Mol. Cell* **1**, 949 (1998).
23. The fusion protein pFkp3–CED-3(205), containing three copies of Fkp fused to CED-3 amino acids 205 to 503, was made in pRK5 as described (*10*). CED-3, CED-3(C358S), CED-4, CED-4 mutants, CED-9, Bcl-x_L, and Apaf-1(1–465) were each fused with a COOH-terminal FLAG epitope tag in pRK5. CED-3(C358S) was also fused to a COOH-terminal AU1 epitope tag in pRK5. Myc–CED-4 and Myc–CED-4 (K165R) were described (*3*). Myc–Apaf-1(1–465) and Myc–CED-3(C358S) were made in pcDNA3.1(-)/MycHis (Invitrogen) with a COOH-terminal Myc tag. Authenticity of each construct was confirmed by DNA sequencing.
24. The day before transfection, 2 × 10^6 293T cells [grown in Dulbecco's minimal essential medium supplemented with 10% fetal bovine serum, penicillin-streptomycin (100 U/ml), and glutamine (1 mM)] were plated per 60-mm dish. Twenty-four hours after transfection by the calcium phosphate method, cells were lysed in 300 μl of IP-lysis buffer [50 mM Hepes (pH 7.4), 1% NP-40, 150 mM NaCl, 10% glycerol, 1 mM EDTA, 2 mM dithiothreitol] supplemented with 1 mM phenylmethylsulfonyl fluoride and 1% aprotinin. Extracts (100 μl) were diluted 1:1 in IP-lysis buffer and immunoprecipitated with antibody for 3 hours at 4°C, washed with 600 μl of IP-lysis buffer, and resolved by SDS–polyacrylamide gel electrophoresis (SDS-PAGE).
25. X. Yang *et al.*, *Cell* **89**, 1067 (1997).

26. We thank F. Chen and H. R. Horvitz for reagents and discussions, P. Svec and A. Darbinian for technical support, and V. M. Dixit, M. Gilman, S. L. Schreiber, and X. Wang for reagents. Supported by the Leukemia Society of America (to X.Y.), the Medical Scientist Training Program (to H.Y.C.), and NIH grant CA51462.

3 June 1998; accepted 13 July 1998

Structure and Asn-Pro-Phe Binding Pocket of the Eps15 Homology Domain

Tonny de Beer, Royston E. Carter, Katherine E. Lobel-Rice, Alexander Sorkin, Michael Overduin*

Eps15 homology (EH) domains are eukaryotic signaling modules that recognize proteins containing Asn-Pro-Phe (NPF) sequences. The structure of the central EH domain of Eps15 has been solved by heteronuclear magnetic resonance spectroscopy. The fold consists of a pair of EF hand motifs, the second of which binds tightly to calcium. The NPF peptide is bound in a hydrophobic pocket between two α helices, and binding is mediated by a critical aromatic interaction as revealed by structure-based mutagenesis. The fold is predicted to be highly conserved among 30 identified EH domains and provides a structural basis for defining EH-mediated events in protein trafficking and growth factor signaling.

Protein interaction domains such as Src homology domains 2 and 3 are devoted to the recruitment of ligands into multiprotein complexes (*1*). The recently discovered EH domain (*2*) is an interaction module that targets NPF-containing proteins such as RAB, NUMB (*3, 4*), clathrin assembly proteins (*5*), and synaptojanin (*6*). Proteins containing these EH domains mediate critical events in endocytosis (*7, 8*) and actin cytoskeletal organization (*8*), and they participate in signaling in conjunction with tyrosine kinases (*2, 9*)

Department of Pharmacology, University of Colorado Health Sciences Center, 4200 East Ninth Avenue, Denver, CO 80262, USA.

*To whom correspondence should be addressed. E-mail: MichaelOverduin@UCHSC.edu

and Src homology domains (*4, 10*). Individual EH repeats consist of about 95 amino acids and have been found in at least 20 proteins in organisms ranging from yeast to mammals (*11*). The prototypic member of this family, Eps15, is made up of an epidermal growth factor receptor (EGFR) phosphorylation substrate that contains three tandem EH domains, binding sites for Crk's Src homology 3 domain (*10*) and clathrin adaptor proteins (*12*), and a coiled-coil oligomerization motif (*13*). Although Eps15 is clearly an essential player in receptor-mediated endocytosis (*7*), it also appears to intersect signaling pathways that regulate cellular growth (*2, 10*), synaptic transmission (*6*), and neuronal development (*14*). The importance of Eps15 is underscored by the discovery of chromosomal translocations involving *eps15* in leukemia (*15*) and of lethal mutations of a yeast *eps15* homolog (*8*). We selected the second EH domain of human Eps15 (EH_2) for structural studies (*16*) because of its putative interactions with NPF-containing proteins (*3*), calcium, and EGFR (*2*) as well as its high degree of sequence conservation.

The structure of EH_2 contains two intimately associated helix-loop-helix motifs connected by a short antiparallel β sheet (Fig. 1). The NH_2-terminal helix αA lies roughly perpendicular to a bundle of the other three α helices (αB, αC, and αD) and primarily contacts the centrally located αD. The helix αC lies diagonally across the parallel αB and αD helices. The tight packing of the helices is reflected in the large number of distance restraints (1795), yielding well-defined solution structures with a root-mean-square deviation (rmsd) of 0.29 ± 0.05 Å for the backbone atoms in secondary structure elements. A proline-rich element following αD zigzags over αC and αD and juxtaposes the NH_2- and COOH-termini. The proximity of these termini would allow the three EH domains of Eps15 to directly abut each other, facilitating cooperative and multivalent binding to ligand proteins.

The peptide motif NPF was recently established as the essential target for the EH domains of Eps15. Binding is enhanced when Thr or Ser occupy the two positions preceding NPF and when a hydrophobic or basic residue follows (*3, 4*). The peptide sequence PTGSSSTNPFL (*17*) contains all of these consensus binding residues and corresponds to the COOH-terminus of RAB, which is a cofactor of the human immunodeficiency virus REV protein. Moreover, the association of RAB and a fusion protein containing EH_2 was previously demonstrated (*3*).

The presence of an exposed binding pocket for this peptide (NPF_{RAB}) is apparent from progressive changes in the ^1H, ^{13}C, and ^{15}N resonances of EH_2 upon titration with NPF_{RAB} (Fig. 2, A and B). Helices αB and αC flank this hydrophobic pocket, which can readily accommodate the NPF residues. The center of the binding site is located approximately 10 Å from the calcium ion and on a face opposite the termini. The bottom of the binding pocket is occupied by Leu^{155}, Leu^{165}, and Trp^{169} (Fig. 2, C and D). The high conservation of the latter two residues and of a hydrophobic residue at the position corresponding to Leu^{155} suggests that they contact the conserved elements in EH domain ligands. The largest chemical shift changes were observed for Leu^{156} and Leu^{165} (Fig. 2B), which implies that they directly contact the Phe side chain of the NPF ligand. The Gly^{148}, Lys^{152}, Val^{162}, and Gly^{166} residues form the edge of the binding pocket, where they may contribute to EH domain specificity.

Because Trp^{169} lies prominently in the NPF binding pocket of EH_2, two mutants were generated in which this amino acid was substituted with either an Ala or a Tyr residue. Both mutants possess a native-like fold, as evident from their ^1H nuclear magnetic resonance (NMR) spectra, which indicates that any change in binding kinetics is directly related to the Trp^{169} mutations. A dissociation constant (K_D) of 560 ± 40 μM was measured for the interaction of wild-type EH_2 with NPF_{RAB}, using surface plasmon resonance detection (*18*). This binding is likely reinforced through multivalent interaction of EH domain clusters with target proteins, which commonly contain multiple NPF motifs (*3–6*). The $Trp^{169} \rightarrow Ala^{169}$ substitution reduced NPF binding beyond detection, demonstrating the critical role of Trp^{169} in NPF binding. In contrast, the $Trp^{169} \rightarrow Tyr^{169}$ substitution reduced the affinity only by a factor of 2.8. The high degree of conservation of this Trp (*2, 11*) and its replacement only by Tyr in a few other EH domains emphasize the importance of the aromatic character of this residue for NPF recognition. Protein interactions involving any EH domain may now be selectively eliminated by mutation of this aromatic residue, allowing the dissection of EH-mediated pathways.

A role for calcium in the activity of EH proteins has been inferred on the basis of the presence of canonical EF hand se-

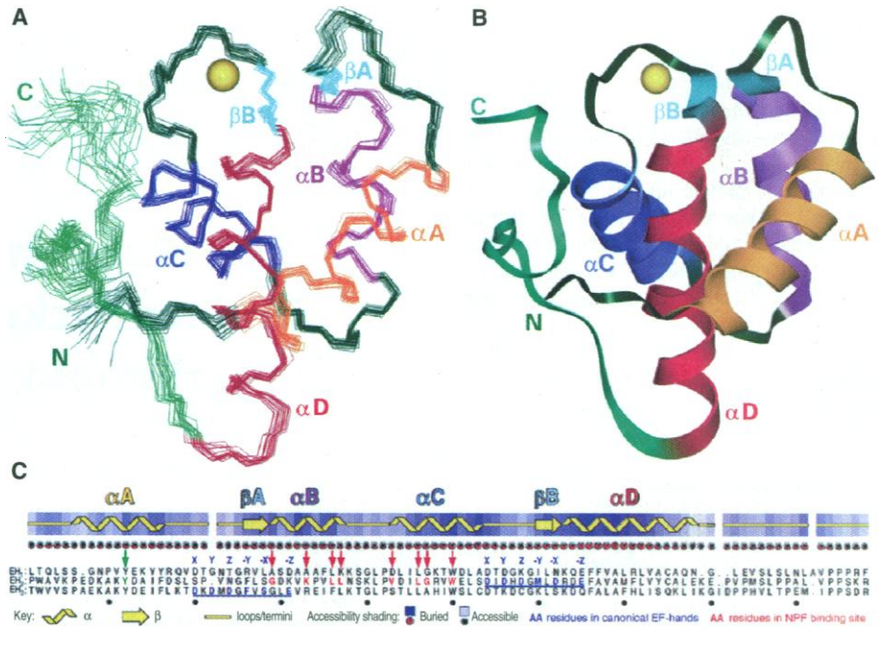

Fig. 1. Structure of EH_2. The four α helices αA (amino acid residues 126 through 136), αB (148 through 156), αC (162 through 172), and αD (182 through 197) are depicted in orange, purple, blue, and red, respectively. The mini–β sheet involving residues 145 through 147 (βA) and 179 through 181 (βB) is shown in light blue, the COOH-terminal proline-rich element is shown in light green, and the calcium ion is shown as a yellow sphere. The NH_2- and COOH-termini are labeled N and C, respectively. Figure 1, A and B, Fig. 2B, and Fig. 3, B and C, were generated with InsightII software. (**A**) Best-fit superposition of the backbone atoms (N, Cα, and C′) in the secondary structure elements of the 20 structures with the lowest nuclear Overhauser effect energies (*21, 22*). (**B**) Ribbon diagram of the structure closest to the average of the 20 structures, shown in the same orientation as (A). (**C**) Amino acid sequence alignment for the three EH domains (residues 9 through 103, 121 through 215, and 217 through 313, respectively) of human Eps15 (*11, 17*). The secondary structure and solvent exposure are shown above the sequence and were determined with Procheck-NMR (*20*). The coloring and nomenclature of key amino acids are indicated in the inset. Phosphorylation of Eps15 at Tyr^{132} (shown in green) by EGFR (*2*) is unlikely because this residue is buried between helices αA and αD.

quence motifs in several EH repeats (*2*). However, calcium binding has not yet been demonstrated, and calcium does not appear to influence Eps15's protein interactions (*2*). Our NMR data pinpoint a binding site for a single calcium ion in the second helix-loop-helix motif of EH_2 (Fig. 3A). The backbone conformation (Fig. 3, B and C) and the amino acid sequence (Fig. 1C) of this loop segment match those of canonical EF hands (*19*), which indicates that calcium is directly ligated by the carboxyl groups of Asp^{173}, Asp^{175}, Asp^{177}, Glu^{184}, and the carbonyl oxygen of Met^{179}. The first helix-loop-helix motif does not bind calcium, but its perpendicular helices and its pairing with the second helix-loop-helix define it as an EF hand variant (Fig. 3, B and C). The loop connecting αA and βA differs most substantially from classical EF hands: it is one residue shorter, contains a Pro residue, and consists of two turns. In light of the EH_2 structure, a calcium ion could be readily accommodated in the first helix-loop-helix in EH domains that bear a canonical EF hand sequence at this position (Fig. 1C). The calcium-bound and free states of EH_2 exhibit slow exchange on the NMR time scale (Fig. 3A). Such tight binding of calcium indicates full occupancy at intracellular calcium concentrations and implies a structural role for calcium rather than a regulatory switch as found in some EF hand proteins (*19*).

Comparison of EH sequences indicates that the structurally critical residues involved in the packing of the hydrophobic core (Fig. 1C) are highly conserved throughout the family. EH domains share the double EF hand fold with other domains within the EF-hand protein superfamily (*19*), but a few notable differences exist. The location of the peptide binding pocket is unprecedented. The αD helix is completely buried within the EH_2 structure and is followed by a proline-rich COOH-terminal element. The modular arrangement and sequence of EH domains further emphasize the fact that these domains constitute a separate class of EF hand proteins. The structure of EH_2 provides a foundation for defining the mechanisms through which

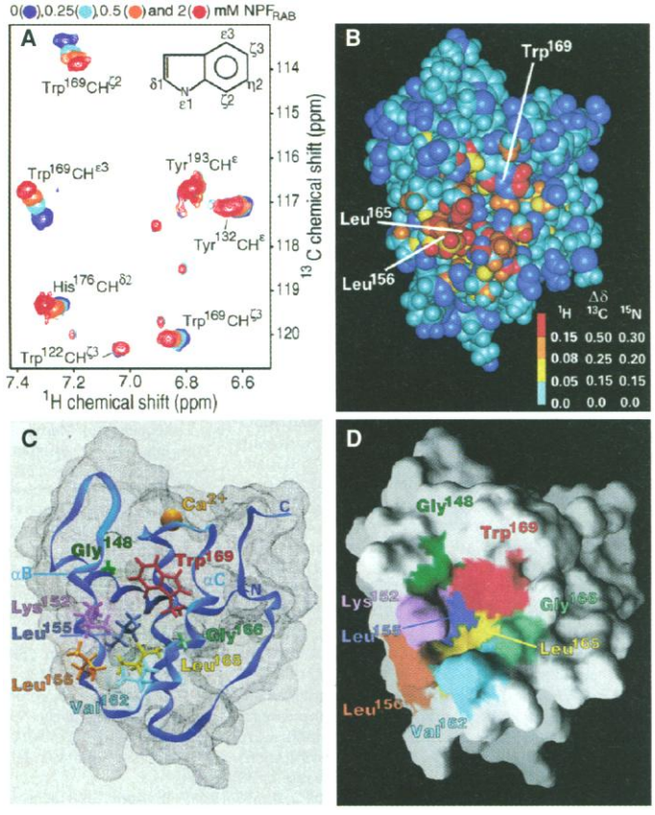

Fig. 2. NPF binding site of EH_2. (**A**) Superimposed regions of four ^{1}H-^{13}C HSQC spectra of 1 mM EH_2 with the following NPF_{RAB} concentrations: 0 mM, dark blue; 0.25 mM, light blue; 0.5 mM, orange; and 2 mM, red. The inset shows the Trp^{169} side chain nomenclature. Observation of fast exchange on the NMR time scale is consistent with the K_D of the EH_2:NPF_{RAB} interaction estimated by surface plasmon resonance (*18*). (**B**) Space-filling model showing the NPF binding site. Atoms are colored on the basis of ^{1}H, ^{13}C, and ^{15}N chemical shift differences (Δδ) induced by NPF_{RAB} addition. Red, orange, yellow, and light blue indicate very large, large, medium, and small differences, respectively, as listed in the inset. Dark blue indicates that the difference was not measured. (**C**) Ribbon diagram displaying side chains in the NPF binding site. The orientation is identical to that in (B). Leu^{155} (dark blue), Leu^{165} (yellow), and Trp^{169} (red) make up the base of the binding site, whereas residues Gly^{148} (dark green), Lys^{152} (magenta), Leu^{156} (orange), Val^{162} (light blue), and Gly^{166} (light green) form the walls of the pocket. Calcium is indicated as a yellow sphere. (**D**) Molecular surface of EH_2 with the same orientation and color coding as in (C) [(C)and (D) were generated with GRASP (*23*)].

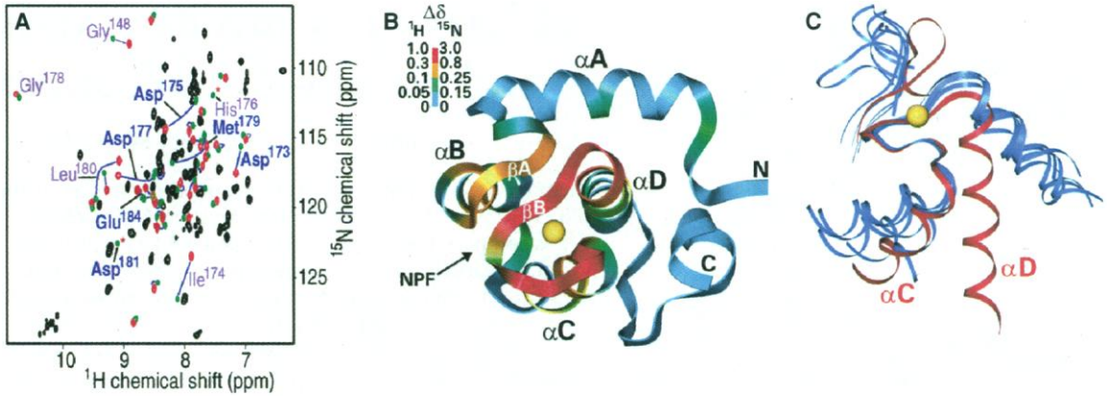

Fig. 3. Calcium binding by EH_2. (**A**) ^{1}H-^{15}N HSQC spectrum of 1 mM EH_2 after EDTA treatment. Pairs of ^{1}H-^{15}N cross peaks belonging to the same amino acid in calcium-bound and free states are colored green and red, respectively, and are connected by blue lines. An asterisk marks ^{1}H-^{15}N cross peaks where only one of the pair could be assigned. Cross peaks of amino acids that did not shift upon calcium removal are drawn in black. Amino acids labeled in blue hold calcium in place through chemical interactions, whereas those in magenta are located in the EF hand loops. (**B**) Ribbon diagram of EH_2 showing the location of the calcium binding site. The ribbon is colored on the basis of ^{15}N, HN, and Hα chemical shift differences (Δδ) between calcium-bound and free states. Red, orange, green, and blue indicate large, medium, small, and negligible chemical shift differences, respectively, as listed in the inset, with the maximum Δδ indicated on top. The yellow sphere represents calcium; the arrow points to the NPF binding site. (**C**) Comparison of the canonical EF hands and paired loops of calmodulin (sites II and IV), troponin C (site II), parvalbumin, calbindin (blue) (*19*), and EH_2 (red). The backbone atoms of the first six residues in the second EF hand loop are superimposed. The helices of the calcium-loaded EF hand of EH_2 are considerably closer than the corresponding helices in the other structures.

this family of domains mediates a host of biological processes, including protein internalization and signaling.

References and Notes

1. T. Pawson and J. D. Scott, *Science* **278**, 2075 (1997).
2. F. Fazioli, L. Minichiello, B. Matoskova, W. T. Wong, P. P. Di Fiore, *Mol. Cell. Biol.* **13**, 5814 (1993); W. T. Wong *et al.*, *Proc. Natl. Acad. Sci. U.S.A.* **92**, 9530 (1995).
3. A. E. Salcini *et al.*, *Genes Dev.* **11**, 2239 (1997).
4. M. Yamabhai *et al.*, in preparation.
5. B. Wendland and S. D. Emr, *J. Cell. Biol.* **141**, 71 (1998).
6. C. Haffner *et al.*, *FEBS Lett.* **419**, 175 (1997).
7. R. Carbone *et al.*, *Cancer Res.* **57**, 5498 (1997); A. Benmerah *et al.*, *J. Cell. Biol.* **140**, 1055 (1998).
8. H. S. Benedetti, F. Paths, F. Crausaz, H. Riezman, *Mol. Biol. Cell.* **5**, 1023 (1994); B. Wendland, J. M. McCaffery, Q. Xiao, S. D. Emr, *J. Cell Biol.* **135**, 1485 (1996).
9. A. Yamaguchi, T. Urano, T. Goi, L. A. Feig, *J. Biol. Chem.* **272**, 31230 (1997); M. Ikeda, O. Ishida, T. Hinoi, S. Kishida, A. Kikuchi, *ibid.* **273**, 814 (1998).
10. C. Schumacher *et al.*, *J. Biol. Chem.* **270**, 15341 (1995).
11. P. P. Di Fiore, P. G. Pelicci, A. Sorkin, *Trends Biochem. Sci.* **22**, 411 (1997).
12. A. Benmerah, B. Begue, A. Dautry-Varsat, N. Cerf-Bensussan, *J. Biol. Chem.* **271**, 12111 (1996).
13. F. Tebar, S. Confalonieri, R. E. Carter, P. P. Di Fiore, A. Sorkin, *ibid.* **272**, 15413 (1997); P. Cupers, E. ter Haar, W. Boll, T. Kirchhausen, *ibid.* **273**, 1847 (1998).
14. V. Avantaggiato, A. Torino, W. T. Wong, P. P. Di Fiore, A. Simeone, *Oncogene* **11**, 1191 (1995).
15. D. Rogaia *et al.*, *Cancer Res.* **57**, 799 (1997).
16. A DNA fragment encoding amino acids 121 through 218 of human Eps15 followed by a TAA stop codon was cloned into the Bam HI and Xho I sites of the pRSETA vector (Clontech). $Trp^{169} \rightarrow Ala^{169}$ and $Trp^{169} \rightarrow Tyr^{169}$ mutations were created by site-directed mutagenesis with the use of the Quick-change system (Stratagene) and were verified by dideoxysequencing. Wild-type EH_2 and mutants were transformed into *Escherichia coli* strains BL21 pLys S and B834 pLys S. Unlabeled or uniformly isotope labeled protein was obtained with LB broth or M9-minimal media containing $^{15}NH_4Cl$ and $^{13}C_6$-glucose. His_6-tagged EH_2 was purified with Talon resin (Clontech) and cleaved with Enterokinase (Novagen), followed by protease removal with EKapture agarose (Novagen). A matrix-assisted laser desorption ionization (MALDI) experiment of imidazole-eluted His_6-tagged EH_2 confirmed the size of 15.45 kD. Amino-terminal sequencing indicated that about 50% of EH_2 lacks the first two amino acids (encoded by the vector), which does not influence the folded structure. EH_2 is monomeric as determined by equilibrium sedimentation ultracentrifugation and pulsed field gradient diffusion experiments [A. S. Altieri, D. P. Hinton, R. A. Byrd, *J. Am. Chem. Soc.* **117**, 7566 (1995)]. All NMR spectra were recorded on samples containing 1 to 4 mM EH_2, 20 mM perdeuterated tris, 0.1 M KCl, 2 mM $CaCl_2$, 0.1 mM perdeuterated dithiothreitol, 10 μM 4-amidinophenylmethane sulfonyl fluoride, and 2 mM NaN_3 (pH = 7.0) dissolved in either 5 or 99.99% $^2H_2O/H_2O$. Calcium binding was assessed from NMR spectra of EH_2 in the presence of calcium and after addition of 10 mM EDTA. Even after repeated EDTA treatment at 37°C, approximately 20% of EH_2 still contained calcium (Fig. 3A). NMR experiments were recorded at 25°C on Varian INOVA 500-MHz and 600-MHz spectrometers equipped with shielded triple resonance probes. NMR experiments [D. R. Muhandiram and L. E. Kay, *J. Magn. Reson. B* **103**, 203 (1994); L. E. Kay, *Biochem. Cell. Biol.* **75**, 1 (1997)] were recorded essentially as described [M. Overduin, K. I. Tong, C. M. Kay, M. Ikura, *J. Biomol. NMR* **7**, 173 (1996)]. Spectra were analyzed with NMRPipe [F. Delaglio *et al.*, *ibid.* **6**, 277 (1995)] and in-house software on Sun Microsystems and Silicon Graphics workstations. Interproton distance restraints (313 intraresidue, 491 sequential, 509 short-range, and 432 long-range) were derived from three-dimensional (3D) and 4D isotope-filtered NOE spectra and were treated as described [C. M. Fletcher, D. N. M. Jones, R. Diamond, D. Neuhaus, *ibid.* **8**, 292 (1996)]. Dihedral restraints including 59 ϕ angles and 45 ψ angles were included based on $^3J_{HN\text{-}H\alpha}$ coupling constants and on $^1H\alpha$, $^{13}C\alpha$, and $^{13}C'$ chemical shifts [D. S. Wishart and B. D. Sykes, *ibid.* **4**, 171 (1994)]. Slowly exchanging amide protons were identified from several $^1H\text{-}^{15}N$ heteronuclear single quantum coherence (HSQC) spectra recorded over a week, after lyophilized protein was dissolved in 99.99% ^2H_2O. In the final calculations, 20 pairs of hydrogen bond restraints were included and six distance restraints between calcium and coordinating oxygen atoms were added, based on average distances in EF hand proteins (*19*). Fifty structures were calculated with the r^{-6} summation method in a restrained molecular dynamics simulated annealing protocol within X-PLOR 3.84 [A. Brünger, *X-PLOR, version 3.1* (Yale Univ. Press, New Haven, CT, 1992)]. Distance and dihedral angle restraints were treated with soft-square-well energy potentials and force constants of 50 kcal mol^{-1} $Å^2$. The total, distance violation, and dihedral violation energies were 307 ± 12 kcal mol^{-1}, 57.0 ± 4.5 kcal mol^{-1}, and 0.68 ± 0.6 kcal mol^{-1}, respectively. No distance and angle restraints were violated by more than 0.35 Å and 2°, respectively. The rmsds from idealized geometry for bonds, angles, and impropers were 0.0028 ± 0.0001 Å, 0.62 ± 0.012°, and 0.47 ± 0.076°, respectively. Ramachandran plot analysis of the 20 structures with Procheck-NMR (*20*) showed that 85.8, 11.3, 2.5, and 0.5% of the non-Gly and non-Pro residues were in the most favorable, additional allowed, generously allowed, and disallowed regions, respectively.
17. Single-letter abbreviations for the amino acid residues are as follows: A, Ala; C, Cys; D, Asp; E, Glu; F, Phe; G, Gly; H, His; I, Ile; K, Lys; L, Leu; M, Met; N, Asn; P, Pro; Q, Gln; R, Arg; S, Ser; T, Thr; V, Val; W, Trp; and Y, Tyr.
18. Approximately 68 resonance units (RU) of NH_2-terminal biotinylated PTGSSSTNPFL (*17*) peptide (Research Genetics) were attached to a streptavidin-coated sensor chip in a BIAcore 2000 instrument. Wild-type EH_2 and the two Trp^{169} mutants were injected over the peptide in eight concentrations ranging from 2 μm to 1.2 mM, with a flow rate of 30 μl min^{-1} in 20 mM Pipes (pH 7.3), 50 mM KCl, 1 mM β-mercaptoethanol, 2 mM $CaCl_2$, 100 μM sodium azide, and 0.005% Tween-20. Equilibrium RU values were estimated at each protein concentration by averaging the steady-state response after injection and correcting for the sample refractive index component. The K_D was estimated from the relation between the EH_2 concentration and equilibrium RU, using steady-state affinity analysis (BIAevaluation 2.1).
19. J. Falke, S. K. Drake, A. L. Hazard, O. B. Peersen, Q. *Rev. Biophys.* **27**, 219 (1994); R. Chattopadhyaya, W. E. Meador, A. R. Means, F. A. Quiocho, *J. Mol. Biol.* **228**, 1177 (1992); N. C. J. Strydnadka *et al.*, *ibid.* **273**, 238 (1997); J. P. Declerq, B. Tinant, J. Parello, J. Rambaud, *ibid.* **220**, 1017 (1991); L. A. Svensson, E. Thulin, S. Forsen, *ibid.* **223**, 601 (1992).
20. R. A. Laskowski, J. A. C. Rullmann, M. W. MacArthur, R. Kaptein, J. M. Thornton, *J. Biomol. NMR* **8**, 477 (1996).
21. Superposition of residues 121 through 215 yields rmsds of 0.54 ± 0.08 Å and 0.92 ± 0.10 Å for the backbone and all heavy atoms, respectively.
22. The disordered five NH_2-terminal residues [DRWGS (*17*)], which are encoded by the expression vector, and the six COOH-terminal residues, which are derived from the third EH domain (KTW) and expression vector (ELI), are not depicted.
23. A. Nicholls, K. A. Sharp, B. Honig, *Proteins* **11**, 281 (1991).

24. We thank R. Muhandiram and L. E. Kay for NMR pulse sequences, J. Mamay for computational support, S. A. Johnson for assistance with BIAcore experiments, P. P. Di Fiori for cDNA, B. Thimmig and C. McHenry for assistance with sedimentation equilibrium experiments, K. Clay and R. Murphy for MALDI data, and J. Enmon, D. Jones, and F. Tebar for insightful discussions. The NMR Center is supported by the Howard Hughes Medical Institute (HHMI). The University of Colorado Cancer Center Facilities for DNA and Protein Sequencing are supported by NIH. This research is funded by NIH and the HHMI (A.S. and M.O.) and by the American Cancer Society and Pew Scholar's Program (M.O.). T.B. and R.E.C. are recipients of NIH and Cancer League of Colorado postdoctoral fellowships, respectively. The coordinates have been deposited in the Brookhaven Protein Data Bank under accession number 1eh2.

30 April 1998; accepted 20 July 1998

Direct Phosphorylation of IκB by IKKα and IKKβ: Discrimination Between Free and NF-κB–Bound Substrate

Ebrahim Zandi,* Yi Chen,* Michael Karin†

A large protein complex mediates the phosphorylation of the inhibitor of κB (IκB), which results in the activation of nuclear factor κB (NF-κB). Two subunits of this complex, IκB kinase α (IKKα) and IκB kinase β (IKKβ), are required for NF-κB activation. Purified recombinant IKKα and IKKβ expressed in insect cells were used to demonstrate that each protein can directly phosphorylate IκB proteins. IKKα and IKKβ were found to form both homodimers and heterodimers. Both IKKα and IKKβ phosphorylated IκB bound to NF-κB more efficiently than they phosphorylated free IκB. This result explains how free IκB can accumulate in cells in which IKK is still active and thus can contribute to the termination of NF-κB activation.

The IKK complex, isolated from extracts of HeLa cells treated with the proinflammatory cytokine TNF (tumor necrosis factor), phosphorylates two regulatory serine residues at the NH_2-termini of the NF-κB inhibitors IκBα and IκBβ (*1*). This phosphorylation event triggers the polyubiquitination of IκBs followed by their degradation through the